[CANCER RESEARCH 61, 2404–2408, March 15, 2001]

Advances in Brief

Vascular Endothelial Growth Factor (VEGF)-C Differentially Affects Tumor Vascular Function and Leukocyte Recruitment: Role of VEGF-Receptor 2 and Host VEGF-A[1]

Ananth Kadambi,[2] Carla Mouta Carreira,[2] Chae-ok Yun,[2] Timothy P. Padera, Dennis E. J. G. J. Dolmans, Peter Carmeliet, Dai Fukumura, and Rakesh K. Jain[3]

Edwin L. Steele Laboratory, Department of Radiation Oncology, Harvard Medical School and Massachusetts General Hospital, Boston, Massachusetts 02114 [A. K., C. M. C., C-o. Y., T. P. P., D. E. J. G. J. D., D. F., R. K. J.], and The Center for Transgene Technology and Gene Therapy, KU Leuven, Leuven B-3000, Belgium [P. C.]

Abstract

Unlike vascular endothelial growth factor (VEGF)-A, the effect of VEGF-C on tumor angiogenesis, vascular permeability, and leukocyte recruitment is not known. To this end, we quantified *in vivo* growth and vascular function in tumors derived from two VEGF-C-overexpressing (VC^+) and mock-transfected cell lines (T241 fibrosarcoma and VEGF-$A^{-/-}$ embryonic stem cells) grown in murine dorsal skinfold chambers. VC^+ tumors grew more rapidly than mock-transfected tumors and exhibited parallel increases in tumor angiogenesis. Furthermore, VEGF-C overexpression elevated vascular permeability in T241 tumors, but not in VEGF-$A^{-/-}$ tumors. Surprisingly, unlike VEGF-A, VEGF-C did not increase leukocyte rolling or adhesion in tumor vessels. Administration of VEGF receptor (VEGFR)-2 neutralizing antibody DC101 reduced vascular density and permeability of both VC^+ and mock-transduced T241 tumors. These data suggest that VEGFR-2 signaling is critical for tumor angiogenesis and vascular permeability and that VEGFR-3 signaling does not compensate for VEGFR-2 blockade. An alternate VEGFR, VEGFR-1 or neuropilin-1, may modulate adhesion of leukocytes to tumor vessels.

Introduction

Members of the VEGF[4] family are known to stimulate endothelial cell migration and proliferation (1, 2). To date, six family members have been identified: VEGF-A, VEGF-B, VEGF-C, VEGF-D, *orf*-VEGF (VEGF-E), and PlGF (1–3). Of these, VEGF-A has been studied most extensively and is known to elevate angiogenesis and permeability in tumors (1, 2) and to increase leukocyte interaction with tumor microvessels (4). In contrast, the effect of VEGF-C on these parameters is not well understood, because direct functional *in vivo* studies on the role of VEGF-C have not been performed. In this study, we tested the hypotheses that VEGF-C increases tumor angiogenesis, vascular permeability, and leukocyte-endothelial cell interactions and further that these effects can be reversed by VEGFR-2 blockade. We transfected two cell lines, T241 fibrosarcoma and V^- ES cells, with a murine VEGF-C construct. Tumors derived from these cells were grown in murine dorsal skinfold chambers and examined by intravital microscopy. VC^+ tumors exhibited increased rates of growth and elevated angiogenesis during the early stages of growth. In addition, we found that both angiogenesis and vessel hyperpermeability were reversible by blockade of VEGFR-2. However, neither VEGF-C overexpression nor VEGFR-2 blockade altered leukocyte-endothelial cell interactions.

Materials and Methods

Cells and Cell Culture. Amphotropic packaging cell lines Phoenix and 293-GPG were provided by Drs. G. P. Nolan (Stanford University Medical Center, Palo Alto, CA) and Richard Mulligan (Children's Hospital, Boston, MA), respectively. T241 murine fibrosarcoma cells were grown in DMEM (Life Technologies, Inc., Grand Island, NY) supplemented with 2 mM L-glutamine, penicillin (100 units/ml), streptomycin (100 μg/ml), and 10% fetal bovine serum (Life Technologies, Inc.) and maintained at 37°C in 5% CO_2. V^- ES cells were cultured as described previously (5).

Cloning of VEGF-C. A cDNA encoding full-length mouse *VEGF-C* was isolated by reverse transcription-PCR from *VEGF-C*-transduced cells. On the basis of the nucleotide sequence of the murine *VEGF-C* gene (DDB/EMBL/GenBank accession no. U73620), *VEGF-C* forward (5′-CCC*GG-ATCCAAGCT*TCCACCATG**G**ACTTGCTGTGCTTCTTGT-3′, incorporating *Bam*HI and *Hin*dIII sites next to the ATG start codon) and *VEGF-C* reverse (5′-TTT*TCTAGAGCGGCCG*CTTAGTTCAGATGTGGCCTTTTCCA-3′, incorporating *Xba*I and *Not*I sites next to the TTA stop codon) primers were designed (restriction sites are *italicized*). For optimization to Kozak's context around the translational start site, the C at position +4 was modified to G (*bold* in the *VEGF-C* forward sequence). PCR amplification resulted in a 1285-bp fragment of full-length *VEGF-C*. This fragment was subcloned using the *Hin*dIII-*Not*I cloning sites of a modified version of the retroviral vector pMMP (a generous gift from Dr. Mulligan), generated in the laboratory of Dr. Brian Seed (Massachusetts General Hospital) by eliminating the original *Hin*dIII site and creating new *Hin*dIII and *Not*I sites within the cloning region. The *VEGF-C* fragment was also subcloned into the *Hin*dIII-*Not*I cloning sites of the pPEAK8 mammalian expression vector (a generous gift from Dr. Seed), generating a pPEAK8-VEGF-C vector.

Creation of VC^+ Cell Lines. For stable transduction of *VEGF-C*, the pMMP vector construct was converted to the corresponding virus as described below. Vector DNA was transfected into helper-free, amphotropic packaging cell lines (Phoenix) and 293-GPG (with similar results) using Ca^{2+}-phosphate transfection in the presence of 25 μM chloroquine. Cultured supernatants from these cells were then harvested. T241 cells were transduced by direct exposure to retroviral supernatants to generate VC^+ cell lines. MT T241 cell lines received empty modified pMMP vector. Following transduction, the viability and number of T241 cells were determined by trypan blue exclusion and hemacytometer counts, respectively. V^- ES cells were transfected with pPEAK8-VEGF-C vector by electroporation, generating V^-VC^+ ES cells. Cells were harvested at log phase, washed twice in cold PBS, and resuspended in PBS at a concentration of 1×10^7 cells/ml. ES cell suspension (500 μl) was added to a cold 4-mm electroporation cuvette containing 10 μg of circular plasmid DNA. Cells and DNA were mixed and incubated on ice for 5 min. Subsequently, a 0.275-kV pulse with capacitance of 975 μF was applied using a Bio-Rad Gene Pulser II. After a 5-min incubation on ice, cells were plated onto a gelatinized 100-mm culture dish. Two days after plating, 2 μg/ml

Received 8/21/00; accepted 1/31/01.

The costs of publication of this article were defrayed in part by the payment of page charges. This article must therefore be hereby marked *advertisement* in accordance with 18 U.S.C. Section 1734 solely to indicate this fact.

[1] Supported by NIH Grant F32-CA83351 (to A. K.), National Cancer Institute Outstanding Investigator Grant R35-CA56591, and NIH Bioengineering Research Partnership Grant R24-CA85140 (to R. K. J.).

[2] These authors contributed equally to this work.

[3] To whom requests for reprints should be addressed, at Department of Radiation Oncology, Massachusetts General Hospital, 100 Blossom Street, Cox-7, Boston, MA 02114. E-mail: jain@steele.mgh.harvard.edu.

[4] The abbreviations used are: VEGF, vascular endothelial growth factor; VEGFR, VEGF receptor; ES, embryonic stem; VD, volumetric density; VC^+, VEGF-C overexpressing; MT, mock-transduced; V^-, VEGF-$A^{-/-}$; mAb, monoclonal antibody; BL, baseline.

puromycine were added for selection. Resistant colonies were picked 2 weeks after electroporation.

Stability of *VEGF-C* Overexpression. To verify that stable overexpression of *VEGF-C* was maintained in tumors during the experiment, Northern blot analysis was performed. A 391-bp mouse *VEGF-C* cDNA probe was generated by PCR using pMMP-VEGF-C as the template (primers: forward, 5′-CAGCACAGGTTACCTCAGCAAGACG; reverse, 5′-GGGTCCACAACTAGATGGCCGAAGC) and used to probe for *VEGF-C* gene expression. Total RNA was isolated from homogenized MT, VC^+, V^-, and V^-VC^+ tumors grown *in vivo* using Ultraspec RNA reagent (BiotechX, Houston, TX) or TRIzol reagent (Life Technologies, Inc.). Hybridization probes were prepared with a random-primed synthesis kit (Rediprime; Amersham Pharmacia Biotech, Piscataway, NJ). Blots were hybridized overnight at 65°C, washed at high stringency (0.1× SCC/1% SDS at 65°C), and exposed on Kodak X-OMAT film.

Determination of VEGF-A Protein Level. Frozen T241 VC^+ and MT tumors (see below) were homogenized in lysis buffer, and total protein was extracted using standard techniques. Total protein was quantified (Bio-Rad DC protein assay kit) according to manufacturer's instructions. ELISA for VEGF-A was performed using the Quantikine M VEGF-A Immunoassay kit (R&D Systems, Minneapolis, MN) following the manufacturer's instructions. Mouse VEGF-A protein included with the kit was used as an internal standard. Reported VEGF-A levels were normalized to the total protein in each sample.

Tumor Model. Dorsal skinfold chambers were surgically implanted in SCID mice of ~30 g of body weight as reported previously (6). Animals were allowed 2–3 days to recover from surgery. Subsequently, 2 μl of dense suspension (containing 2×10^5 T241 VC^+ or MT tumor cells, or V^-VC^+ or V^- ES cells) were injected into the striated muscle layer of the remaining s.c. tissue (6). Tumors were excised when they filled the chamber (surface area of ~75 mm^2), immediately snap-frozen in liquid nitrogen, and stored at −70°C for molecular and protein analysis. An additional set of T241 VC^+ and MT tumors was harvested before the end point of the study (day 10 of tumor growth) for VEGF-A ELISA.

Intravital Microscopy. Tumor-bearing animals were anesthetized with a mixture of ketamine and xylazine, placed on a microscope stage (Zeiss Axioplan), and observed under high power. Using FITC-dextran contrast-enhancement (Sigma Chemical Co.; molecular weight, 2,000,000; 10 mg/ml), images of tumor microvessels were acquired with an Intensified Charged Coupled Device (ICCD) camera (AVC D7; Sony, Tokyo, Japan) and digitized on a Macintosh 8100 computer with NIH image software (version 1.6). Tumor surface area, the area of the top surface of the tumor within the dorsal chamber, and VD, the average vessel volume contained in five high-power fields of the tumor, were measured off-line as described previously (7). The vascular permeability coefficient was measured using cyanine-5 (Amersham Pharmacia Biotech)-labeled BSA (Sigma Chemical Co.), as described previously (8). For visualization of leukocyte-endothelial cell interactions, animals received i.v. injections of 20 μl of 0.1% rhodamine 6-G (Sigma Chemical Co.) in 0.9% saline and images were videotaped (S-VHS VCR model SVO-9500 MD; Sony) for off-line analysis. RBC velocity was measured using temporal correlation velocimetry, and microvessel shear rates were calculated as described in Ref. 6. The total leukocyte flux (N_t), number of rolling (N_r), and number of adherent (N_a) leukocytes along 100-μm segments of converging vessels were counted over 30 s (8). Adherent leukocytes were classified as those that remained stationary for >10 s.

VEGFR-2 Blockade. Intravital microscopy was performed in T241 VC^+- or MT-tumor bearing animals treated with the rat antimouse VEGFR-2 function-blocking mAb DC101 (9). DC101 mAb (1.2 mg; ImClone, Inc.) was administered i.p. every 3 days (7), immediately following the intravital microscopy measurement for that day. Tumors were size-normalized (*i.e.*, the BL tumor size for both VC^+ and MT ranged between 50 and 60 mm^2). Most tumors grew to fill the visible part of the dorsal chamber (surface area of ~75 mm^2) 3 days after the initiation of treatment. Hence, a two-dimensional area was not measurable beyond this point. A separate group of control animals bearing MT and VC^+ tumors were treated with control mAb (1.2 mg, rat IgG against mouse IgA; ImClone, Inc.) on the same treatment schedule. Tumors were rapidly harvested following the last intravital microscopy measurement, snap-frozen, and stored at −70°C for molecular analysis. Because of their slow growth and the limited lifetime of the dorsal skinfold chamber, VEGFR-2 blockade experiments were not performed on V^-VC^+ or V^- tumor-bearing animals.

Statistics. Population means were tested for significant differences by the two-tailed Student's *t* test. Significance was assumed when $P < 0.05$. All data are presented as mean ± SEM unless otherwise noted.

Results and Discussion

VEGF-C RNA Is Elevated in VC^+ Tumors. Northern analysis of T241 VC^+ and MT tumor lysates using equal amounts of RNA in each lane and equal exposure times yielded the two bands expected with the pMMP-based construct in VC^+ but not MT tumors (Fig. 1, *left*). The pMMP vector (Maloney full *GAG* vector-based) generates two RNA transcripts as a result of alternative splicing outside the *VEGF-C* construct. Although both transcripts contain the full-length *VEGF-C* cDNA, translation of the shorter species is typically more efficient (10). Northern analysis of V^-VC^+ tumor lysates yielded a single band of ~1.8 kb, as expected with the pPEAK8-based construct (Fig. 1, *right*). Western blot analysis showed a result consistent with overproduction of VEGF-C by T241 VC^+ cell and tumor lysates (data not shown).

VEGF-C Overexpression Augmented Tumor Angiogenesis, Vascular Permeability, and Growth. VEGF-C has been shown to mediate vascular function in nonneoplastic settings, including *in vitro* capillary endothelial cell proliferation and migration, *in vivo* angiogenesis (11), and vascular permeability (12). In this study, T241 tumors overexpressing VEGF-C exhibited a significant increase in tumor growth and in angiogenesis during the early stages of tumor growth (Fig. 2, *a–d*). Quantitative analysis confirmed that T241 VC^+ tumor surface area was significantly elevated over MT tumors at days 10 and 13 after implantation (Fig. 2*e*) before reaching the limit of the assay at day 16. Furthermore, VD, an index of angiogenesis, exhibited an ~4-fold increase at day 10 in T241 VC^+ tumors and a 3-fold increase at day 13 (Fig. 2*f*). Both vessel diameter and length were elevated in T241 VC^+ tumors (data not shown). Vascular permeability achieved a significant 2-fold increase in T241 VC^+ tumors at day 13 (Fig. 2*g*). Similar increases in tumor angiogenesis and vascular permeability due to VEGF-C overexpression were also observed in

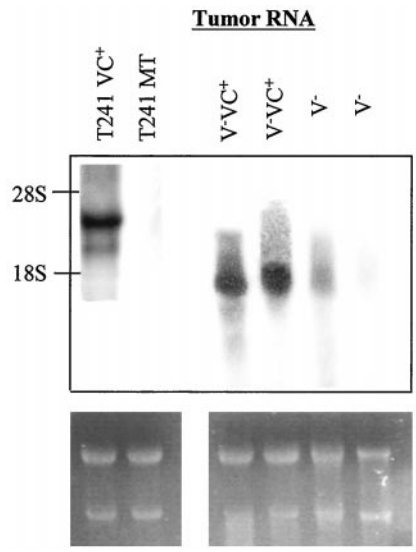

Fig. 1. Northern analysis of VC^+ tumor lysates. *Top*, VEGF-C mRNA is undetectable in T241 MT tumors (*left*). Two bands of 3.4 (*top*) and 2.4 kb (*bottom*) are evident between 18S and 28S rRNAs in VC^+ tumors, as expected with pMMP vector. These bands correspond to the full-length transcript and a splice product lacking ~1 kb of viral non-long terminal repeat regions. VEGF-C mRNA is detectable as a single, 1.8-kb band in V^-VC^+ tumors (*right*), the full-length transcript expected with the pPEAK8 vector. *Bottom*, ethidium bromide-stained gels for analysis of total RNA loading and integrity.

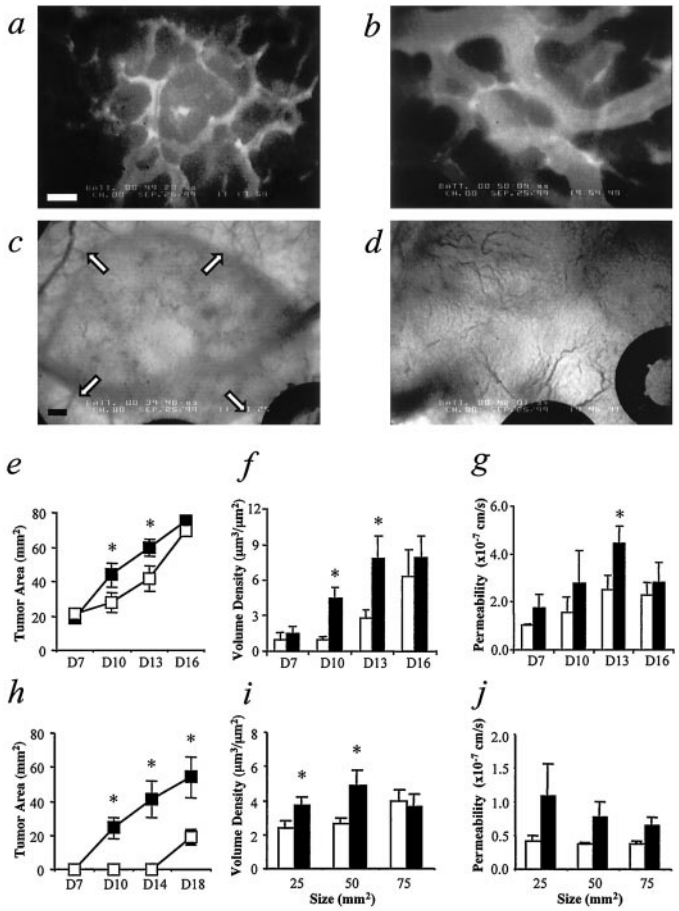

Fig. 2. Rapid-onset angiogenesis and growth in VC^+ tumors. *a-d*, two-dimensional growth and angiogenesis of T241 MT and VC^+ tumors 13 days after implant in the dorsal skinfold chamber, with FITC-dextran contrast enhancement of microvessels (*a* and *b*) or low-power transillumination (*c* and *d*). MT tumors (*a* and *c*) exhibit relatively little growth, as the tumor boundary is visible within the image (*arrows*), and vessels are of relatively small diameter. In contrast, VC^+ tumors (*b* and *d*) exhibit significant growth, as the tumor boundary is not visible within the image, and several vessels of relatively large diameter are evident. *Bars*, 50 μm (*a* and *b*) and 250 μm (*c* and *d*). *e-j*, quantification of functional vascular parameters. *e*, two-dimensional surface area of T241 VC^+ tumors rose significantly faster than MT tumors over the measurement period. *f*, VD, an index of angiogenesis, was 4-fold greater in VC^+ tumors than MT tumors at *D10* and 3-fold greater at *D13*. *g*, vascular permeability was significantly higher in VC^+ tumors at *D13*. *h*, two-dimensional surface area of tumors derived from V^-VC^+ ES cells increased significantly faster than that of tumors derived from V^- ES cells at early stages of growth. Furthermore, the mean total time required for tumors to fill the visible area of the dorsal chamber (area, 75 mm^2) was significantly lower in V^-VC^+ tumors (26 $\pm$ 4.2 days *versus* 45 $\pm$ 3.4 days, $P < 0.01$). *i*, VD in V^-VC^+ tumors was significantly elevated at smaller sizes. *j*, no significant differences in vascular permeability were observed between V^-VC^+ and V^- tumors, but permeability in V^-VC^+ tumors trended higher at all measured sizes. □, T241 MT or V^-; ■, T241 VC^+ or V^-VC^+; *, $P < 0.05$ as compared with corresponding MT tumors (n = 5–7 animals for T241, 4–6 for ES).

B16F10 melanoma, another rapidly growing tumor line (data not shown).

To determine whether endogenous VEGF-A accounted for the observed differences, ELISA for murine VEGF-A was performed. At days 10 and 16 of tumor growth, comparable levels of VEGF-A protein were observed in T241 VC^+ and MT tumors. MT tumors contained 294 $\pm$ 64 pg/mg VEGF-A at day 10 and 347 $\pm$ 58 pg/mg at day 16, whereas VC^+ tumors contained 350 $\pm$ 47 pg/mg VEGF-A at day 10 and 394 $\pm$ 84 pg/mg at day 16. Differences were not significant between the groups at either time point.

Although significant differences in vascular function were observed between T241 VC^+ and MT tumors during early growth (time-matched comparison), comparison of functional parameters in size-matched T241 VC^+ and MT tumors yielded no significant difference between the two groups. Therefore, we hypothesized that the effects of VEGF-C may be dependent on VEGF-A protein level or tumor growth rate. Hence, we may have been unable to detect differences in functional parameters in size-matched T241 tumors due to their rapid growth or the influence of tumor-derived VEGF-A. To test this hypothesis, we studied the effects of VEGF-C on slowly growing teratomas derived from V^- ES cells. A prior study of V^- teratomas indicated that they contain 50% of VEGF-A found in wild-type teratomas (presumably produced by host cells within the tumor), grow slower, and exhibit lower vascular density, permeability, and leukocyte adhesion (4). Our data show that overexpression of VEGF-C in V^- cells was able to partially "rescue" the V^- phenotype. Differences in tumor growth rate between V^-VC^+ and control tumors during early stages of growth were quite pronounced (Fig. 2*h*), and time-matched analysis during the early growth rate was not possible for this reason. However, size-matched analysis showed that V^-VC^+ tumors exhibited significantly elevated VD during the early stages of growth (25 mm^2 and 50 mm^2). Vascular permeability of V^-VC^+ tumors, however, was not significantly elevated at any measured size (Fig. 2, *i–j*). Hence, in the teratomas, which grew much more slowly than the T241 fibrosarcomas, similar effects on tumor angiogenesis were observed on VEGF-C overexpression even under size-matched analysis. Collectively, our data support the hypothesis that differences in levels of VEGF-C, not only in VEGF-A, can account for increases in tumor growth and facilitate tumor angiogenesis (13, 14). The effects of VEGF-C on tumor vascular permeability, however, remain unclear and are discussed further below.

Blockade of VEGFR-2 Reversed Angiogenesis. Whereas VEGF-A binds VEGFR-1 (flt-1) and VEGFR-2 (flk-1/KDR), VEGF-C binds VEGFR-2 and VEGFR-3 (flt-4; Ref. 3). Although VEGFR-2 signaling dominates VEGF-A function, it is not clear which receptor is important for VEGF-C-induced angiogenesis. The mAb DC101 specifically binds murine VEGFR-2.[5] Here, we show that administration of DC101 to mice bearing established, size-matched T241 VC^+ and MT tumors elicited significant vessel regression (Fig. 3, *a* and *b*). Although the size of tumors in all four groups increased slightly (Fig. 3*c*), the limit of the assay (75 mm^2) does not allow us to fully interpret the effect of VEGFR-2 blockade on tumor growth. VD in both DC101-treated groups was significantly lower than IgG-treated groups by 6 days after initiation of treatment (Fig. 3*d*, *D6*). In the IgG-treated groups, VD continued to increase beyond BL, achieving significance at D3 for both IgG groups; however, in the DC101-treated groups, VD became lower than BL and undetectable at later time points. No significant difference in VD was observed between established, size-matched DC101-treated MT and VC+ groups at any time point regardless of the treatment. Collectively, our data implicate VEGFR-2 as a primary mediator of tumor angiogenesis, confirming earlier reports (1–3). Although we found detectable levels of VEGFR-3 in our tumors by reverse transcription-PCR (data not shown), the VEGF-C-VEGFR-3 pathway did not rescue angiogenesis after DC101 treatment.

In summary, although significant efforts, to date, have focused on blockade of VEGF-A and its receptors as a means of antiangiogenic therapy, our data collectively suggest that blockade of VEGFR-2, which binds both VEGF-A and VEGF-C, may be superior to blockade of VEGF-A alone in the treatment of tumors. Furthermore, the rapid vascular regression we observed in both tumor groups may be a result of blockade of both VEGF-A and VEGF-C signaling via VEGFR-2. In light of recent data showing that administration of soluble VEGFR-3 reduces angiogenesis mediated by VEGF-C via VEGFR-2

[5] D. J. Hicklin, personal communication.

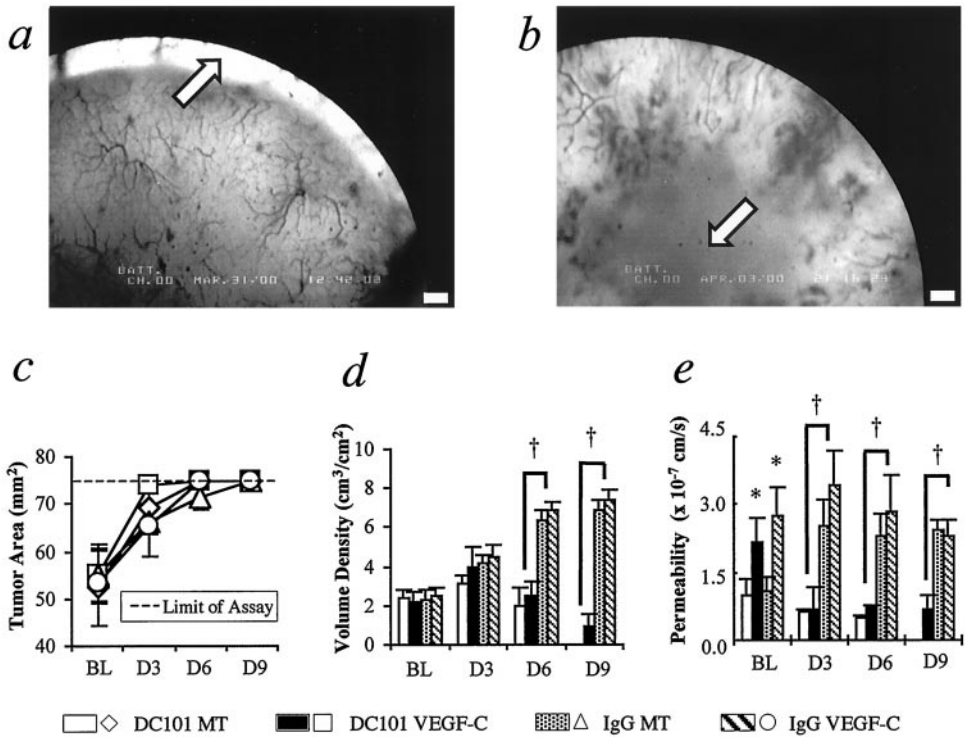

Fig. 3. Effects of VEGFR-2 blockade by DC101 mAb administration. Five to seven T241 tumors in each group were size-matched at BL, and treatment with DC101 or control IgG was begun. Analysis was performed every 3 days after treatment onset (*D3*, *D6*, and *D9*). *a* and *b*, representative transillumination images of the same tumor 3 days (*a*) and 6 days (*b*) after DC101 treatment. *a*, normal tissue is seen outside the tumor boundary (*arrow*), along with distinct vasculature. Significant vascular regression has occurred in *b*, but tumor growth has continued to a maximum quantifiable size. A large, avascular area is visible toward the tumor center (*b*, *arrow*; *bar*, 500 μm). *c*, tumor growth in all groups continued normally after DC101 administration up to *D3*. After *D6*, tumors of all groups filled the dorsal window, maximum measurable area of which is 75 mm^2 (*dashed line*), precluding further quantification of growth beyond this size. *d*, VD was not significantly different between the DC101-treated VC$^+$ and MT tumors up to *D3*. However, VD in both DC101-treated tumor groups was significantly lower than IgG-treated tumor groups at *D6* and *D9* (†, $P < 0.01$). In the IgG-treated groups, VD became significantly greater than BL at *D3* (*, $P < 0.05$) and continued to increase to the study end point. *e*, vascular permeability was ~2-fold higher in VC$^+$ tumors relative to their respective MT controls at BL (*, $P < 0.05$). Permeability in DC101-treated tumor groups exhibited a sharp reduction by *D3*, and was significantly decreased compared with IgG-treated groups at all successive time points (†, $P < 0.05$, all) but not significantly different from the MT BL level.

(15), we propose that the quantity of VEGFR-3 present on the tumor vascular endothelium may be critical to tumor angiogenesis facilitated by the VEGF-C-VEGFR-2 pathway. This possibility remains to be explored.

Blockade of VEGFR-2 Reversed Vascular Hyperpermeability. Elevated permeability is a hallmark of tumor microvasculature (16–18). The VEGF family, and VEGF-A in particular, is known to mediate the hyperpermeability of tumor vessels (1–3). A role for VEGF-C in modulating vascular permeability has been demonstrated *in vitro* and via Miles assay *in vivo* (12, 19). Furthermore, VEGF-C has been shown to act synergistically with VEGF-A to induce degradation of matrix components (14) and angiogenesis *in vitro* (15). In our study, BL vascular permeability was significantly greater in T241 VC$^+$ tumors than in MT tumors (Fig. 3*e*), but permeability in both VC$^+$ tumors and MT tumors declined to the levels of normal vessels (~5 $\times$ 10^{-8} cm/s) 3 days after the initiation of DC101 treatment. Furthermore, these levels were maintained for the remainder of the study. Permeability could not be measured at D9 in treated MT tumors because functional vessels could not be detected (Fig. 3*d*). No difference in vascular permeability was observed between established, size-matched IgG-treated VC$^+$ and MT tumors at any time point following the initiation of IgG administration, but permeability in both IgG-treated groups was significantly greater than DC101-treated groups. These findings suggest that tumor microvascular permeability is predominantly mediated by VEGFR-2 in our model.

The vascular permeability of MT tumors, presumably a result of VEGF-A (16, 18), decreases to the limit of detection following VEGFR-2 blockade. The functional data derived from our time-matched and size-matched analysis of T241 tumors (Figs. 2*g* and 3*e*) suggest that VEGF-C overexpression increases vascular permeability beyond that induced by VEGF-A alone. However, the V$^-$ tumor permeability data (Fig. 2*j*) argue against this hypothesis. The relative difference in VEGF-C protein expression between T241 VC$^+$ and V$^-$VC$^+$ tumors is unknown due to the lack of sufficiently sensitive quantitative assays; hence, the possibility exists that the discrepancy is a simple result of increased VEGF-C production by T241 VC$^+$ tumors. However, if the tumors produce similar levels of VEGF-C, three alternate explanations of this discrepancy are also consistent with our data. First, VEGF-C may act directly to increase vascular permeability via VEGFR-2, independently of VEGF-A. Second, VEGF-A and VEGF-C may act synergistically via VEGFR-2 (14). In this case, we would expect a decreased permeability in MT tumors after VEGFR-2 blockade mainly due to loss of VEGF-A-VEGFR-2 signal, but would expect VC$^+$ tumor permeability to decrease to a greater extent due to loss of both synergy and VEGF-A signaling. Third, VEGF-C may potentiate VEGF-A-VEGFR-2-induced increases in vascular permeability via VEGFR-3. The VEGF-C-VEGFR-3 effect, however, may not be observed in the absence of the VEGFR-2 signaling pathway, and blockade of VEGFR-2 would, thus, completely eliminate hyperpermeability. A quantification of vascular permeability in normal tissue treated with variable quantities of VEGF-C and VEGF-A protein may illuminate the interplay between these growth factors in the modulation of tumor vascular permeability.

VEGF-C Overexpression Did Not Affect Leukocyte-Endothelial Cell Interactions. Inflammatory cytokines induce VEGF-C expression, and it has been proposed that this may influence lymphocyte

Table 1 *Leukocyte-endothelial cell interactions in T241 VC$^+$ and MT tumors*

Group[a]	Tumor type[b]	N_t (cells/30 s)[c]	N_r (%)[d]	N_a (cells/mm^2)[e]
BL	*MT*	8.0 ± 1.4	22.3 ± 4.6	75.7 ± 39.9
	VC$^+$	9.0 ± 1.5	17.4 ± 3.5	63.2 ± 43.9
D3	*MT DC101*	11.0 ± 1.6	19.3 ± 3.4	146.3 ± 46.7
	VC$^+$ DC101	6.0 ± 1.6	14.3 ± 4.4	80.1 ± 65.6
	MT IgG	8.5 ± 1.8	15.0 ± 6.1	95.3 ± 47.5
	VC$^+$ IgG	9.0 ± 2.1	20.4 ± 3.6	112.4 ± 51.4
D6	*MT DC101*	14.0 ± 2.6	14.7 ± 4.0	137.9 ± 37.9
	VC$^+$ DC101	11.0 ± 2.0	19.7 ± 4.7	143.1 ± 56.0
	MT IgG	13.5 ± 1.8	15.8 ± 3.9	85.5 ± 51.4
	VC$^+$ IgG	16.0 ± 2.0	18.5 ± 5.1	101.3 ± 61.9

[a] D3, 3 days post-DC101 treatment initiation; D6, 6 days post-DC101 treatment initiation.
[b] *DC101*, DC101-treated; *IgG*, nonspecific rat IgG-treated.
[c] Total leukocyte flux/30 s.
[d] Percentage of rolling leukocytes.
[e] Number of adherent leukocytes/mm^2. Data are mean ± SEM.

trafficking in inflammation (20). However, the effects of VEGF-C on leukocyte recruitment and adhesion to endothelium have not been characterized, to date. In contrast to other parameters associated with angiogenesis, we found that leukocyte-endothelial interactions as characterized by total leukocyte flux, rolling percentage, and adhesion density were not significantly different between size-matched T241 VC^+ and MT tumors before or after treatment with DC101 (Table 1), in age-matched T241 VC^+ and MT tumors (data not shown) or in size-matched V^- teratomas (data not shown). DC101-treated tumors did not exhibit significantly different leukocyte-endothelial interactions compared with the IgG-treated groups (Table 1). Microvessel shear rates were not significantly different between any groups (data not shown). Interestingly, VEGF-C sufficient to produce significant and detectable increases in vascular permeability (compared with normal tissue) seemed to be present in BL VC^+ tumors (Fig. 3*e*), but the same VEGF-C expression did not produce a detectable increase in leukocyte recruitment. Furthermore, in V^-VC^+ tumors that contain ~50% of control tumor VEGF-A (4), no detectable increase in leukocyte recruitment is observed (data not shown), suggesting that VEGF-C alone does not mediate leukocyte-endothelium interaction. In light of data demonstrating that VEGF-A may recruit leukocytes to sites of inflammation via up-regulation of endothelial intercellular adhesion molecule-1 or vascular cell adhesion molecule-1 (21), these observations further suggest that leukocyte adhesion molecule up-regulation may be modulated via a receptor other than VEGFR-2, such as VEGFR-1 (flt-1) or neuropilin-1 (22). However, detectable effects on leukocyte recruitment following VEGFR-2 blockade may not have been observed because of low BL leukocyte infiltration in these tumors. These possibilities remain to be explored. In conclusion, given the wide variety of human tumors known to express VEGF-C (3, 23), our findings suggest that VEGF-C may play a critical role in the angiogenesis, hyperpermeability, and growth of human tumors.

Acknowledgments

We thank Dr. Kari Alitalo for help with reagents, Dr. Dan Hicklin for generously providing DC101, Julia Kahn for dorsal chamber preparation and tumor cell implantation, Drs. Brian Seed and Winfried Pickl for providing the modified pMMP retroviral vector and pPEAK8 mammalian vector, Dr. Rahmi Oklü for assistance with Northern blot analysis, and Drs. Lance Munn and Saroja Ramanujan for helpful comments.

References

1. Carmeliet, P., and Jain, R. K. Angiogenesis in cancer and other diseases. Nature (Lond.), *407:* 249–257, 2000.
2. Ferrara, N. Molecular and biological properties of vascular endothelial growth factor. J. Mol. Med., *77:* 527–543, 1999.
3. Veikkola, T., Karkkainen, M., Claesson-Welsh, L., and Alitalo, K. Regulation of angiogenesis via vascular endothelial growth factor receptors. Cancer Res., *60:* 203–212, 2000.
4. Tsuzuki, Y., Fukumura, D., Oosthuyse, B., Koike, C., Carmeliet, P., and Jain, R. K. Vascular endothelial growth factor (VEGF) modulation by targeting hypoxia-inducible-factor-1α 63 HRE 63 VEGF cascade differentially regulates vascular response and growth rate in tumors. Cancer Res., *60:* 6248–6252, 2000.
5. Carmeliet, P., Ferreira, V., Breier, G., Pollefeyt, S., Kieckens, L., Gertsenstein, M., Fahrig, M., Vandenhoeck, A., Harpal, K., Eberhardt, C., Declercq, C., Pawling, J., Moons, L., Collen, D., Risau, W., and Nagy, A. Abnormal blood vessel development and lethality in embryos lacking a single VEGF allele. Nature (Lond.), *380:* 435–439, 1996.
6. Leunig, M., Yuan, F., Menger, M. D., Boucher, Y., Goetz, A. E., Messmer, K., and Jain, R. K. Angiogenesis, microvascular architecture, microhemodynamics, and interstitial fluid pressure during early growth of human adenocarcinoma LS174T in SCID mice. Cancer Res., *52:* 6553–6560, 1992.
7. Hansen-Algenstaedt, N., Stoll, B. R., Padera, T. P., Dolmans, D. E. J. G. J., Hicklin, D. J., Fukumura, D., and Jain, R. K. Tumor oxygenation in hormone-dependent tumors during vascular endothelial growth factor receptor-2 blockade, hormone ablation, and chemotherapy. Cancer Res., *60:* 4556–4560, 2000.
8. Fukumura, D., Yuan, F., Endo, M., and Jain, R. K. Role of nitric oxide in tumor microcirculation. Blood flow, vascular permeability, and leukocyte-endothelial interactions. Am. J. Pathol., *150:* 713–725, 1997.
9. Witte, L., Hicklin, D. J., Zhu, Z., Pytowski, B., Kotanides, H., Rockwell, P., and Bohlen, P. Monoclonal antibodies targeting the VEGF receptor-2 (Flk1/KDR) as an anti-angiogenic therapeutic strategy. Cancer Metastasis Rev., *17:* 155–161, 1998.
10. Krall, W. J., Skelton, D. C., Yu, X. J., Riviere, I., Lehn, P., Mulligan, R. C., and Kohn, D. B. Increased levels of spliced RNA account for augmented expression from the MFG retroviral vector in hematopoietic cells. Gene Ther., *3:* 37–48, 1996.
11. Witzenbichler, B., Asahara, T., Murohara, T., Silver, M., Spyridopoulos, I., Magner, M., Principe, N., Kearney, M., Hu, J. S., and Isner, J. M. Vascular endothelial growth factor-C (VEGF-C/VEGF-2) promotes angiogenesis in the setting of tissue ischemia. Am. J. Pathol., *153:* 381–394, 1998.
12. Joukov, V., Sorsa, T., Kumar, V., Jeltsch, M., Claesson-Welsh, L., Cao, Y., Saksela, O., Kalkkinen, N., and Alitalo, K. Proteolytic processing regulates receptor specificity and activity of VEGF-C. EMBO J., *16:* 3898–3911, 1997.
13. Valtola, R., Salven, P., Heikkila, P., Taipale, J., Joensuu, H., Rehn, M., Pihlajaniemi, T., Weich, H., deWaal, R., and Alitalo, K. VEGFR-3 and its ligand VEGF-C are associated with angiogenesis in breast cancer. Am. J. Pathol., *154:* 1381–1390, 1999.
14. Pepper, M. S., Mandriota, S. J., Jeltsch, M., Kumar, V., and Alitalo, K. Vascular endothelial growth factor (VEGF)-C synergizes with basic fibroblast growth factor and VEGF in the induction of angiogenesis *in vitro* and alters endothelial cell extracellular proteolytic activity. J. Cell. Physiol., *177:* 439–452, 1998.
15. Hamada, K., Oike, Y., Takakura, N., Ito, Y., Jussila, L., Dumont, D. J., Alitalo, K., and Suda, T. VEGF-C signaling pathways through VEGFR-2 and VEGFR-3 in vasculoangiogenesis and hematopoiesis. Blood., *96:* 3793–3800, 2000.
16. Yuan, F., Chen, Y., Dellian, M., Safabakhsh, N., Ferrara, N., and Jain, R. K. Time-dependent vascular regression and permeability changes in established human tumor xenografts induced by an anti-vascular endothelial growth factor/vascular permeability factor antibody. Proc. Natl. Acad. Sci. USA, *93:* 14765–14770, 1996.
17. Hobbs, S. K., Monsky, W. L., Yuan, F., Roberts, W. G., Griffith, L., Torchilin, V. P., and Jain, R. K. Regulation of transport pathways in tumor vessels: role of tumor type and microenvironment. Proc. Natl. Acad. Sci. USA, *95:* 4607–4612, 1998.
18. Dvorak, H. F., Nagy, J. A., Feng, D., Brown, L. F., and Dvorak, A. M. Vascular permeability factor/vascular endothelial growth factor and the significance of microvascular hyperpermeability in angiogenesis. Curr. Top. Microbiol. Immunol., *237:* 97–132, 1999.
19. Joukov, V., Kumar, V., Sorsa, T., Arighi, E., Weich, H., Saksela, O., and Alitalo, K. A recombinant mutant vascular endothelial growth factor-C that has lost vascular endothelial growth factor receptor-2 binding, activation, and vascular permeability activities. J. Biol. Chem., *273:* 6599–6602, 1998.
20. Ristimaki, A., Narko, K., Enholm, B., Joukov, V., and Alitalo, K. Proinflammatory cytokines regulate expression of the lymphatic endothelial mitogen vascular endothelial growth factor-C. J. Biol. Chem., *273:* 8413–8418, 1998.
21. Melder, R. J., Koenig, G. C., Witwer, B. P., Safabakhsh, N., Munn, L. L., and Jain, R. K. During angiogenesis, vascular endothelial growth factor and basic fibroblast growth factor regulate natural killer cell adhesion to tumor endothelium. Nat. Med., *2:* 992–997, 1996.
22. Giraudo, E., Primo, L., Audero, E., Gerber, H. P., Koolwijk, P., Soker, S., Klagsbrun, M., Ferrara, N., and Bussolino, F. Tumor necrosis factor-α regulates expression of vascular endothelial growth factor receptor-2 and of its co-receptor neuropilin-1 in human vascular endothelial cells. J. Biol. Chem., *273:* 22128–22135, 1998.
23. Leu, A. J., Berk, D. A., Lymboussaki, A., Alitalo, K., and Jain, R. K. Absence of functional lymphatics within a murine sarcoma: a molecular and functional evaluation. Cancer Res., *60:* 4324–4327, 2000.

Vascular Endothelial Growth Factor (VEGF)-C Differentially Affects Tumor Vascular Function and Leukocyte Recruitment: Role of VEGF-Receptor 2 and Host VEGF-A

Ananth Kadambi, Carla Mouta Carreira, Chae-ok Yun, et al.

Cancer Res 2001;61:2404-2408.